A HUMAN MODELING APPROACH FOR EFFICIENT COMPUTER ANIMATION

D.M. EMIRIS[†], G. STAVRAKAKIS[†], A.POULIEZOS[‡],
A.C. IORDANIDIS [†] and C. PNEVMATIKATOS [†]

Robotics and Automation Laboratory
Department of Electronics and Computer Engineering
Technical University of Crete
73100 Chania, GREECE

e-mail: emiris@dilos.ced2.tuc.gr

Abstract —*Human modeling is an intrinsic problem in computer animation applications. Human beings which interact with their environment are often involved in complex animation scenes. The quality of an animation sequence is directly influenced by the choice of the human model. This paper focuses on the kinematic aspect of human modeling for walking applications and proposes an algorithmic animation scheme for body-motion control. The problem of proper human modeling is resolved by using two classes of articulated robot geometries, namely, the elbow and the dual-elbow, to model the arms and legs, respectively. The resulting model exploits the properties of the two geometries, the symmetric nature of the human motion, and the parallelism in its implementation, in order to minimize the associated computational complexity. A rendering module is developed to depict the animation sequence on a computer screen. The motion of the human is shown to be smooth, and to satisfy the imposed joint and contact constraints.*
Keywords: *Human modeling, optimal robot geometries, algorithmic computer animation, ray-tracing.*

Manuscript submitted to the Eurographics 94 Conference; January 11th, 1994.

[†] Department of Electronics and Computer Engineering.

[‡] Department of Production and Engineering Management.

1 Introduction

Human modeling is an intrinsic problem in computer animation applications. Human beings which interact with their environment are often involved in complex animation scenes [1]. The quality of an animation sequence is directly influenced by the choice of the human model. Human modeling typically refers to the construction of an articulated structure that assimilates the human body and that is able to perform most of the movements of a real person. Proper human modeling improves the natural aspect of motion and increases the realism of an animation scene. Although animation scenes involve, in general, "clothed skeletons", significant work has been done on animation involving "naked" articulated structures. Most animation of clothed structures is controlled by animating an underlying skeleton of some description and then completing the final images with flesh and/or clothes [2].

Several approaches to human modeling for animation have appeared in the recent years in the literature [3, 4, 5, 6]. The proposed models possess a different number of degrees-of-freedom (DOF), depending on the application they were designed for; most of these applications involve human walking. Motion of these models is performed by employing kinematic and/or dynamic strategies to control the motion parameters; these approaches however, present high computational load and cannot be executed in real-time [7, 8, 9]. Walking is the fundamental form of human motion; human models employ walking to move in their environments and to create the conditions for interaction with other models or objects. The study of human walking, furthermore, is particularly attractive because of the existing inherent symmetries and the hierarchical interaction between the subsystems that compose the human body.

This paper focuses on the kinematic aspect of human modeling for walking applications. Walking sequences necessitate motion of almost all the elements of the human body with respect to a world frame or to the body itself. The problem addressed herein is thus to construct a human model that most precisely reflects the physical and behavioral characteristics of a real person during walking, and to develop a computationally-efficient body-motion control strategy.

The present approach resolves the problem of proper human modeling by using robotic geometries to model the limbs of the human. Specifically, two classes of articulated robot geometries with six degrees-of-freedom each, namely, the *elbow* and the *dual-elbow*, are employed to model the arms and legs, respectively. Both geometries are anthropomorphic; the first three axes in the elbow configuration form the positioning "arm" and the last three form the orienting "wrist". The dual-elbow geometry is the kinematic inverse of the elbow geometry in the sense that the positioning "arm" and the orienting "wrist" of the latter are interchanged in the kinematic chain. The two geometries have been proven to be optimal in the sense that they maximize the work volume for a given total link length [10, 11]; furthermore, they are decoupled and they provide closed-form, analytic solutions to the inverse kinematics problem [12].

These geometries are combined herein to create a hierarchical system based on anthropometric data, and then, to develop a kinematic control scheme for the calculation of the joint parameters during walking, and which behaves smoothly in the neighborhood of singular positions. The resulting strategy exploits the properties of the two geometries, the symmetric nature of the human motion, and the parallelism in its implementation, in order to minimize the associated computational complexity. This scheme requires only these parameters that specify the speed of the walk and the number of steps performed.

The motion of the model is planned at the task level, that is, in world (cartesian) coordinates rather than in joint coordinates; in other words, it is an *algorithmic* animation and *not* a *keyframe* animation scheme. This choice was made for two reasons. First, it is more natural, in the sense that real humans decide and coordinate their movements to interact with their environment in the cartesian level rather than in the joint level; a human, for example, knows that he/she needs to lift his/her leg by a certain amount to climb a staircase, instead of calculating the relative displacement of each joint in the leg separately. Secondly, it is more difficult and expensive to gather data (e.g. from rotoscopy) for each joint – especially when joints are not simple (e.g. spherical) – and/or when the motion of the human is not trivial.

The performance of the present algorithm has been tested and scrutinized. A rendering module to depict the animation sequence in the computer has been developed. A human model based on ellipsoidal limbs was adopted, the number of which depends on the degrees-of-freedom in the kinematic representation, while their shape reflects the dimensions according to anthropometric data. The resulting figurines are described by mathematical equations to simplify rendering procedures; the algorithm used for their production presents acceptable speed and representation quality. The motion of the human is smooth, and satisfies the imposed joint constraints *and* the floor constraints (that is, there is no foot penetration on the floor). Hidden surface removal and shading are accomplished with ray tracing.

This paper is organized as follows. In Section 2, the ideal elbow and dual-elbow robotic geometries are presented. In Section 3, the realistic versions of the ideal robotic geometries are employed to construct the integrated human model. A complete kinematic study of these geometries is performed herein. In Section 4, the problems of trajectory planning and of the motions of the distinct subsystems are addressed in turn. Then, in Section 5 a paradigm of motion of the human model reveals the efficiency of the current implementation. Finally, in Section 6, the contributions of this paper are summarized and areas for future research are highlighted.

2 Ideal Articulated Geometries

In this section, the ideal elbow and dual-elbow articulated robot geometries are presented. These geometries are employed in this paper to model the limbs of the human model. Specifically, the elbow geometry is used to model the human arms, and the dual-elbow geometry is used to model the legs. In the sequel, the two geometries are described in the robotics context.

2.1 The Elbow Geometry

Elbow manipulators are general-purpose anthropomorphic devices consisting of six rotational joints. The first three joints constitute the robotic "arm", while the remaining three form the robotic "wrist" on which the end-effector is attached. The arm is primarily responsible for positioning the end-effector in space, while the wrist is primarily responsible for orienting it. The following formal definition of an ideal elbow manipulator is an edited version of the one introduced by Paden [13].

Definition 2.1.1 *A robot manipulator with six rotational joints is an elbow manipulator, if there exists a configuration* $\mathbf{q} = (\theta_1, \theta_2, \ldots, \theta_6)^T$ *at which* (Figure 1)*:*

- $\mathbf{z}_0$ *and* $\mathbf{z}_1$ *intersect perpendicularly at point B;*
- $\mathbf{z}_1$ *is parallel to* $\mathbf{z}_2$*;*
- $\mathbf{z}_3$, $\mathbf{z}_4$ *and* $\mathbf{z}_5$ *are mutually orthogonal and co-intersect at point H;*
- $\mathbf{z}_1$ *is perpendicular to the line segment BH; and*
- $\mathbf{z}_2$ *is the perpendicular bisector of BH.*

In the above definition, $\mathbf{z}_i$ $(i = 1, \ldots, 6)$ denote the axes of motion (rotation), while θ_i $(i = 1, \ldots, 6)$ are the joint displacements. From the definition of the elbow manipulator it can be inferred that the length L_1 of the second link (the *upper arm*), and the length L_2 of the third link (the *forearm*), are both equal to L. Furthermore, the axes $\mathbf{z}_3, \mathbf{z}_4$ and $\mathbf{z}_5$ form a spherical joint. *The ideal elbow geometry is therefore decoupled.* The tool axis $\mathbf{z}_6$ in an ideal elbow geometry coincides with axis $\mathbf{z}_5$, with the origin of the end-effector coordinate frame located at a distance $L_3(= L_t)$ from the center of the spherical wrist. The axis arrangement in an ideal elbow geometry provides the robot with the capability of a base rotation about $\mathbf{z}_0$, a shoulder rotation about $\mathbf{z}_1$, an elbow rotation about $\mathbf{z}_2$, and wrist rotations about $\mathbf{z}_3$, $\mathbf{z}_4$, and $\mathbf{z}_5$.

The assignment of coordinate frames to an ideal elbow manipulator is performed using the Denavit-Hartenberg convention. The Denavit-Hartenberg parameters of the ideal elbow geometry are summarized in Table 1. It is observed that in the elbow manipulator geometry the twist angles are either 0° or 90° for each link, and that each link has either a zero length d_i or a zero joint offset r_i.

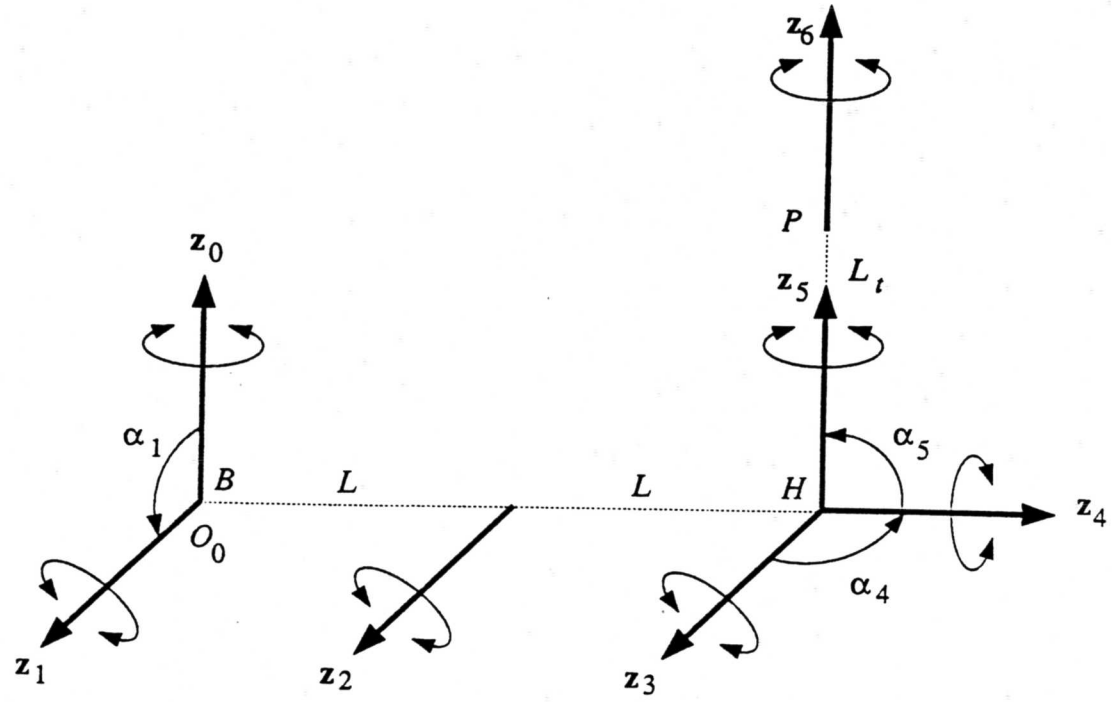

Figure 1: *Definition of the Ideal Elbow Manipulator Geometry.*

Link i	θ_i	r_i	d_i	α_i
1	θ_1	0	0	$-90°$
2	θ_2	0	L_1	$0°$
3	θ_3	0	L_2	$0°$
4	θ_4	0	0	$-90°$
5	θ_5	0	0	$-90°$
6	θ_6	L_3	0	$0°$

Table 1: *Denavit-Hartenberg Parameters for an Ideal Elbow Manipulator.*

The inverse kinematics problem for the ideal elbow geometry consists of computing the joint coordinates (θ_1, θ_2, θ_3, θ_4, θ_5, θ_6) required to place the end-effector in a desired pose in space. For the elbow manipulator geometry, motion of any of the intersecting joints $\mathbf{z}_3$, $\mathbf{z}_4$, and $\mathbf{z}_5$, does not affect the position of the co-intersection point H, and therefore, the positioning task is decoupled. The inverse kinematics problem for the elbow manipulator, therefore, is demoted to the problem of solving for the three joint coordinates θ_1, θ_2, and θ_3 required to position the co-intersection point. Then, these values are used in combination with the task description, to formulate a lower-order system where the only unknowns are the last three joint coordinates, θ_4, θ_5, and θ_6; for this system closed-form solutions also exist. The complete inverse kinematics solution for an ideal elbow manipulator is presented analytically in [14].

For a certain position of the hand, the elbow can have two configurations; elbow up, where the elbow's position is above the line BH joining the shoulder and the wrist; and elbow down, where the elbow's position is below that line. Furthermore, depending upon the value of the joint angle θ_1, the manipulator may represent a left arm, or a right arm configuration. Finally, depending upon the value of the joint angle θ_5, the wrist can be in a no-flip wrist configuration, or a flip wrist configuration. Thus, for a desired pose of the end-effector, there exist up to eight different joint displacements sets to achieve it. In a real-time application, the control computer selects at each time-instant the solution set that is the nearest neighbor to the solution at the previous time-instant.

The singularities of the manipulator represent the boundaries between the solutions to the inverse kinematics problem [15, 16]. At a singularity, infinite joint velocities are required to maintain a finite end-effector velocity; in effect, the manipulator is unable to move along (or around) certain directions [17]. The existence of singular positions *inside* the robot workspace is an inherent problem for task planning and robot control [18, 19].

For an ideal elbow manipulator, there exist three singularities. At the first singular configuration, $\sin\theta_3 = 0$ and the robotic arm is either fully contracted or fully extended. At the second singularity, $\cos\theta_2 + \cos(\theta_2 + \theta_3) = 0$ and the intersection point H of the axes $\mathbf{z}_3$, $\mathbf{z}_4$, and $\mathbf{z}_5$ lies on the $\mathbf{z}_0$ axis and thus a rotation about this axis is compensated by the motion of the spherical wrist; one degree-of-freedom is then lost. Finally, at the third singular configuration, $\sin\theta_5 = 0$ and axes $\mathbf{z}_3$ and $\mathbf{z}_5$ are aligned; θ_4 and θ_6 describe the same rotation; one degree-of-freedom is thus lost. It should be observed that the manipulator singularities consist of exactly the arm singularities and the wrist singularities; that is, the positional ability of the arm is not affected by the loss of an orientational degree-of-freedom; similarly, the orientational ability of the wrist is not affected by the loss of a positional degree-of-freedom.

2.2 The Dual-Elbow Geometry

Dual-elbow manipulators are articulated robots consisting of six rotational joints. The ideal dual-elbow geometry is the kinematic inverse of the ideal elbow geometry in the sense that the positioning "arm" and the orienting "wrist" of the latter are interchanged in the kinematic chain. The following formal definition of an ideal dual-elbow manipulator is an edited version of the one introduced by Paden [13].

Definition 2.2.1 *A robot manipulator with six rotational joints is a dual-elbow manipulator, if there exists a configuration* $\mathbf{q} = (\theta_1, \theta_2, \ldots, \theta_6)^T$ *at which* (Figure 2)*:*
- $\mathbf{z}_0$, $\mathbf{z}_1$ *and* $\mathbf{z}_2$ *are mutually orthogonal and co-intersect at point B;*
- $\mathbf{z}_4$ *and* $\mathbf{z}_5$ *intersect perpendicularly at point H;*
- $\mathbf{z}_3$ *is parallel to* $\mathbf{z}_4$*;*
- $\mathbf{z}_4$ *is perpendicular to the line segment BH; and*
- $\mathbf{z}_3$ *is the perpendicular bisector of BH.*

From the definition of the dual-elbow geometry it can be inferred that the length L_1 of the third link the length L_2 of the fourth link are both equal to L. Furthermore, the axes $\mathbf{z}_0, \mathbf{z}_1$ and $\mathbf{z}_2$ form a spherical joint. *The ideal dual-elbow geometry is therefore decoupled.* The tool axis $\mathbf{z}_6$ coincides with axis $\mathbf{z}_5$, with the origin of the end-effector coordinate frame located at a distance L_3 (equal to the *tool length* L_t) from the center of the spherical joint. The axis arrangement in the ideal dual-elbow geometry provides the robot with the capability of a spherical motion about the base joint axes $\mathbf{z}_0$, $\mathbf{z}_1$ and $\mathbf{z}_2$, a rotation about $\mathbf{z}_3$, and forward rotations about $\mathbf{z}_4$ and $\mathbf{z}_5$.

The assignment of coordinate frames to an ideal dual-elbow manipulator follows the Denavit-Hartenberg convention. The Denavit-Hartenberg parameters of the dual-elbow geometry are summarized in Table 2. It is observed that, as in the elbow manipulator geometry, the twist angles are either 0° or 90° for each link, and that each link has either a zero length d_i or a zero joint offset r_i.

For the dual-elbow manipulator geometry, motion of any of the intersecting joints $\mathbf{z}_0$, $\mathbf{z}_1$, and $\mathbf{z}_2$, does not affect the position of the co-intersection point B as seen from the end-effector. The inverse kinematics problem for the dual-elbow manipulator, therefore, is demoted to the problem of solving for the three joint coordinates θ_4, θ_5, and θ_6 required to position the co-intersection point B, when the task is described in the end-effector frame. Then, these values are used in combination with the task description, to formulate a lower-order system where the only unknowns are the first three joint coordinates; for this system closed-form solutions also exist. The complete inverse kinematics solution for an ideal dual-elbow manipulator is presented analytically in [14].

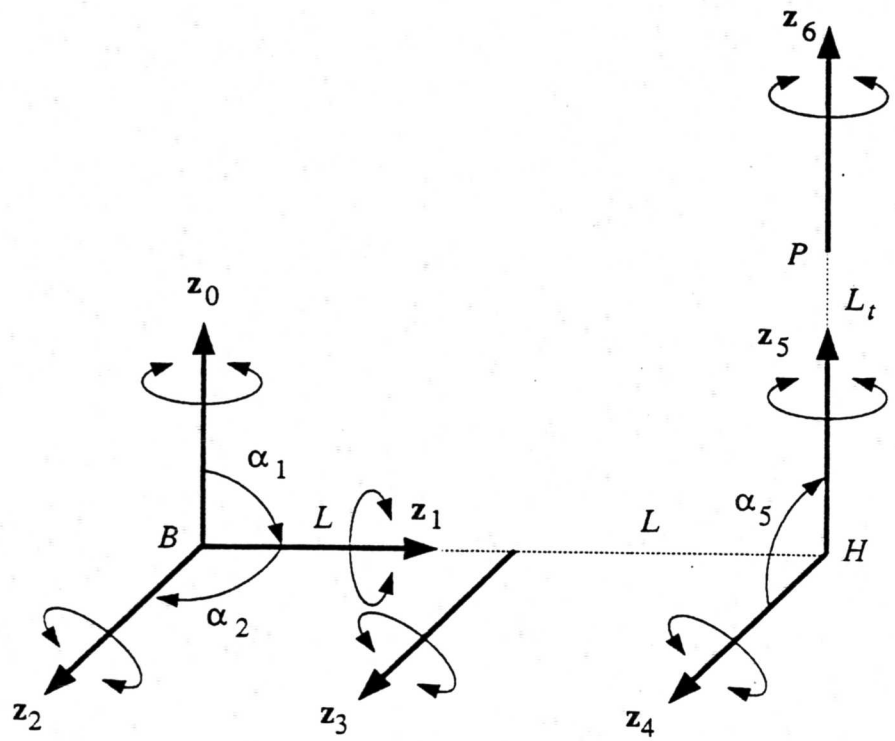

Figure 2: *Definition of the Ideal Dual-Elbow Manipulator Geometry.*

Link i	θ_i	r_i	d_i	α_i
1	θ_1	0	0	$-90°$
2	θ_2	0	0	$-90°$
3	θ_3	0	L_1	$0°$
4	θ_4	0	L_2	$0°$
5	θ_5	0	0	$-90°$
6	θ_6	L_3	0	$0°$

Table 2: *Denavit-Hartenberg Parameters for an Ideal Dual-Elbow Manipulator.*

For a certain position of the end-effector, the dual-elbow can have two configurations; elbow up, where the origin of the third frame is above the line segment BH joining the shoulder and the wrist; and elbow down, where the origin of the third frame is below that line. Furthermore, depending upon the value of the joint angle θ_2, the manipulator may represent a left hand, or a right hand configuration. Finally, depending upon the value of the joint angle θ_6 the wrist can be in a no-flip wrist configuration, or a flip wrist configuration. Thus, for a desired position of the end-effector, there exist up to eight different joint displacements sets to achieve it. In a real-time application, the control computer selects at each time-instant the solution set that is the nearest neighbor to the solution at the previous time-instant.

The dual-elbow manipulator has a decoupled robot geometry and thus guarantees singularity decoupling. The manipulator singularities, therefore, consist of exactly the positional singularities and the orientational singularities. Since there are eight distinct solutions, in general, to the inverse kinematics problem, there exist three robotic singularities. At the first singular configuration, $\sin\theta_4 = 0$ and the robotic arm is either fully contracted or fully extended. At the second singularity, $\cos\theta_5 + \cos(\theta_4 + \theta_5) = 0$ and the intersection point B of the axes $\mathbf{z}_0$, $\mathbf{z}_1$, and $\mathbf{z}_2$, lies on the $\mathbf{z}_5$ axis and rotation about this axis is compensated by the motion of the spherical joint; one degree-of-freedom is then lost. Finally, at the third singularity, $\sin\theta_2 = 0$ and axes $\mathbf{z}_0$ and $\mathbf{z}_2$ are aligned; θ_1 and θ_3 describe the same rotation; one degree-of-freedom is thus lost.

2.3 Realistic Robot Geometries

The formal definitions of the ideal elbow and dual-elbow geometries presented herein, have shown that the one constitutes the inverse kinematic mapping of the other, in the sense that the "arm" and the "wrist" are interchanged in the kinematic chain [12]. Indeed, the kinematic parameters of the i-th link of the one are identical to the kinematic parameters of the $(6-i)$-th link of the other, for $i = 1, \ldots, 5$; the absolute values of the twist angles are either 0° or 90°; each link has either a zero length or a zero joint offset; the forearm and the upper arm have the same length; and the joints are assumed to have complete rotational freedom [11, 20].

Realistic robot geometries arise because of designed deviations from the ideal case and because of unavoidable manufacturing errors [21, 22]. The realistic geometries employed in this paper are characterized by the following deviations:

- Unequal upper arm and forearm lengths for both geometries, and
- Presence of joint limits at every joint for both geometries.

These constraints are imposed in order to model the limbs of the human model as accurately as possible . In this context, the link lengths and the joint limits are derived from anthropometric data reflecting the body structure.

3 The Human Model for Walking

In this section, the skeleton of the human model is described and the subsystems that compose it are highlighted. Then, the realistic elbow and dual-elbow geometries are incorporated in the human model and their specific characteristics are outlined.

3.1 The Skeleton of the Human Model

The skeleton of the human model consists of six distinct subsystems, namely, the right and left legs (denoted by $\{\mathcal{L}^R\}$ and $\{\mathcal{L}^L\}$, respectively), the right and left arms (denoted by $\{\mathcal{A}^R\}$ and $\{\mathcal{A}^L\}$, respectively), the main body (which includes the thorax and the clavicles and is denoted by $\{\mathcal{B}\}$), and the head (which includes the neck and is denoted by $\{\mathcal{H}\}$). These systems are depicted in Figure 3.

The head subsystem consists of a spherical joint able of turning the head left or right, and up or down, and also to bend it to the left or right (Figure 4). The head is connected to the main body with the *neck* link. The four limbs subsystems consist of six joints each. The legs are connected between them by the *waist* link, while the arms are connected between them by the *back* link. The main body subsystem consists of three joints that move the *vertebrae* links. These enable the rotation of the *waist* link about ${}^{\mathcal{B}}\mathbf{z}_0$, and about an axis parallel to ${}^{\mathcal{B}}\mathbf{y}_0$, and the *back* link about ${}^{\mathcal{B}}\mathbf{z}_0$. The main body subsystem coincides the human model system. The motion of the human model in space can be specified as a motion of the main body subsystem in space; furthermore, any motion of this system causes the other subsystems to move as well.

3.2 The Human Legs Model

The legs of the humanoid are modeled upon the realistic dual-elbow geometry; that is, there exist joint limits reflecting limited rotational capabilities of the human leg joints, while the lengths L_1 and L_2 are specified from anthropometric data. The coordinate frames for the legs are depicted in Figure 5a.

The ${}^{\mathcal{L}}\mathbf{z}_0$ axis points vertically upwards along the feet-head direction; rotation about this axis corresponds to a hip *flexion*. Axis ${}^{\mathcal{L}}\mathbf{x}_0$ points towards the direction of motion and is always parallel to the world ${}^{\mathcal{W}}\mathbf{x}_0 - {}^{\mathcal{W}}\mathbf{y}_0$ plane for human walking applications. The ${}^{\mathcal{L}}\mathbf{y}_0$ axis completes the right-hand frame. Typically, in a walking sequence, the orientation of the $\{\mathcal{L}^R\}$ and $\{\mathcal{L}^L\}$ frames relative to the body and the world systems remains constant; changes in the direction of motion result from changes in the orientation of the body system. Rotation about ${}^{\mathcal{L}}\mathbf{z}_3$ corresponds to knee bending, while rotations about ${}^{\mathcal{L}}\mathbf{z}_4$, and ${}^{\mathcal{L}}\mathbf{z}_5$ correspond to ankle motions. The origin of the foot coordinate system (equivalent to the end-effector frame) coincides with the foot tip, while the ${}^{\mathcal{L}}\mathbf{z}_6$ axis is perpendicular to the foot and points away from the floor and the ${}^{\mathcal{L}}\mathbf{x}_6$ axis lies along the foot direction and points towards the toes.

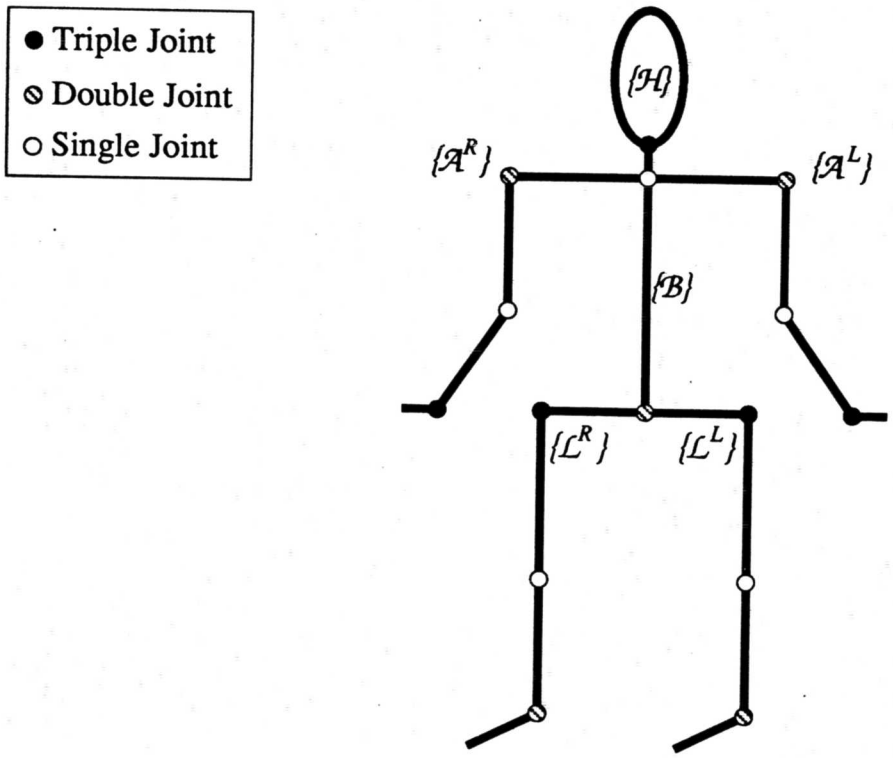

Figure 3: *Definition of the Human Model Skeleton.*

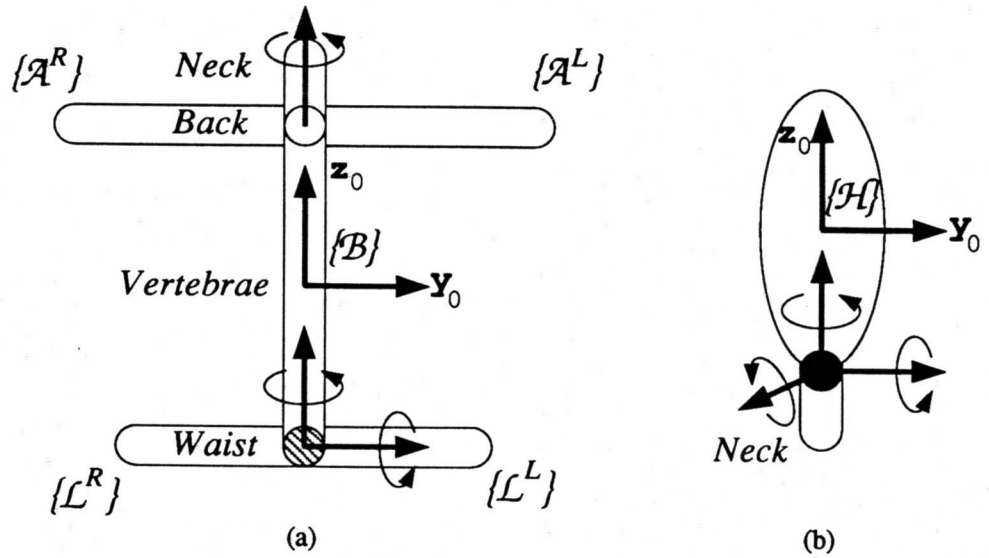

Figure 4: *Definition of the Main Body and Head Coordinate Systems.*

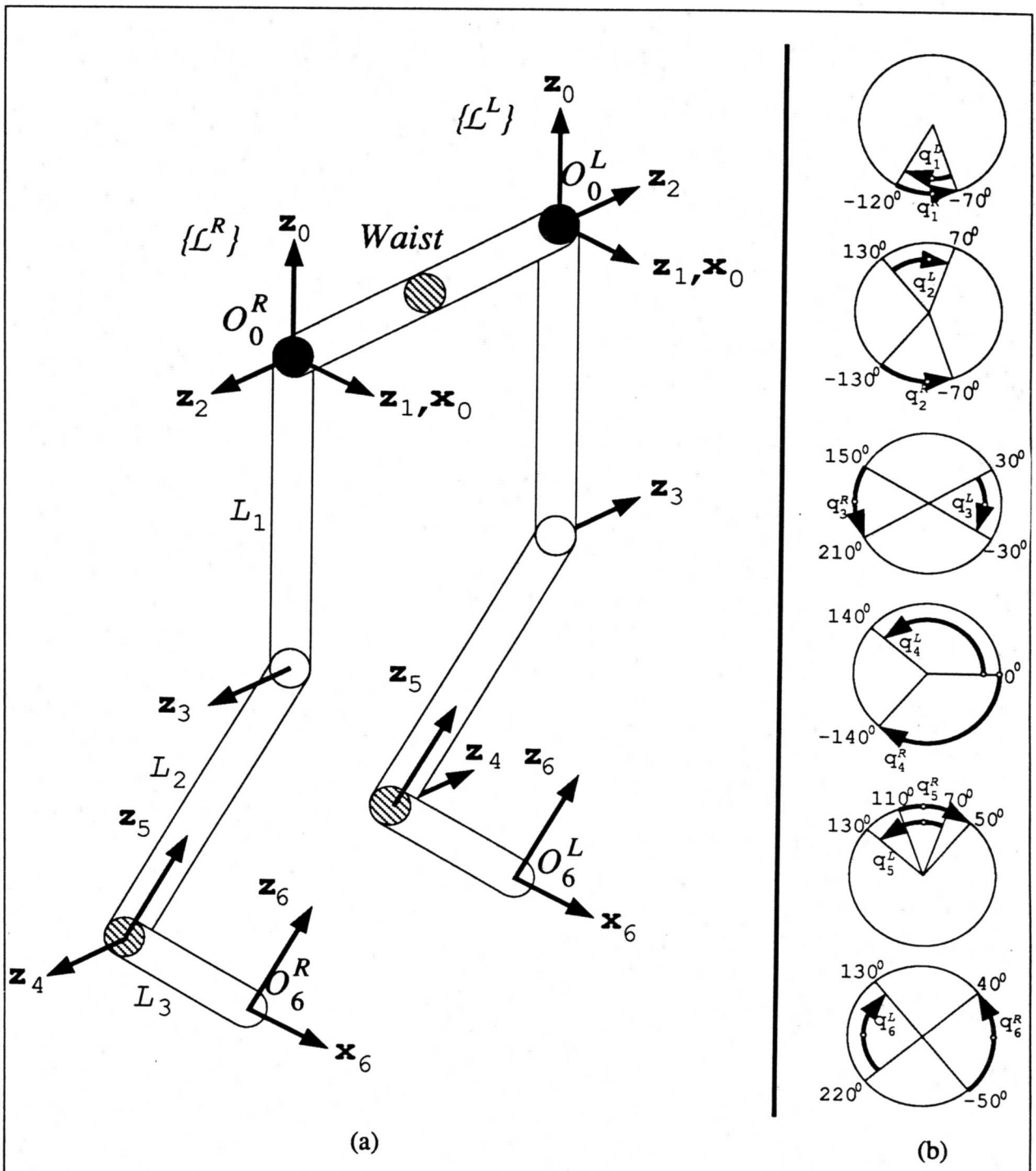

Figure 5: *(a) Definition of the Left and Right Legs Coordinate Systems. (b) The Range of Motion of the Leg Joints.*

The range of motion of each joint in the legs model is depicted in Figure 5b, where the superscripts R and L denote the joint variables for the right and left legs, respectively. White dots in this figure indicate the values of the joint variables at the zero position, which occurs when the human model is standing (not walking). The direction of the arrows indicates how the same joint variable in the left and right legs varies in order to produce the same leg motion. The absolute amount of freedom for each joint is identical for both legs. The joint variable ${\theta_4}^R$, for example, varies from 0° to −140° while ${\theta_4}^L$ varies from 0° to 140° to produce the same amount of flexion at the knees.

The joint limits are employed to limit the solution space in the computation of the inverse kinematics solution for each leg at a desired pose. For example, since $-140° \leq \theta_4^R \leq 0°$ ($0° \leq \theta_4^L \leq 140°$) for the right (left) leg, $\sin\theta_4^R \leq 0$ ($\sin\theta_4^L \geq 0$) always; otherwise the leg will be forced to assume an abnormal position. Similarly, it follows that always $\sin\theta_2^R < 0$ ($\sin\theta_2^L > 0$) and that $\cos\theta_6^R > 0$ ($\cos\theta_6^L < 0$).

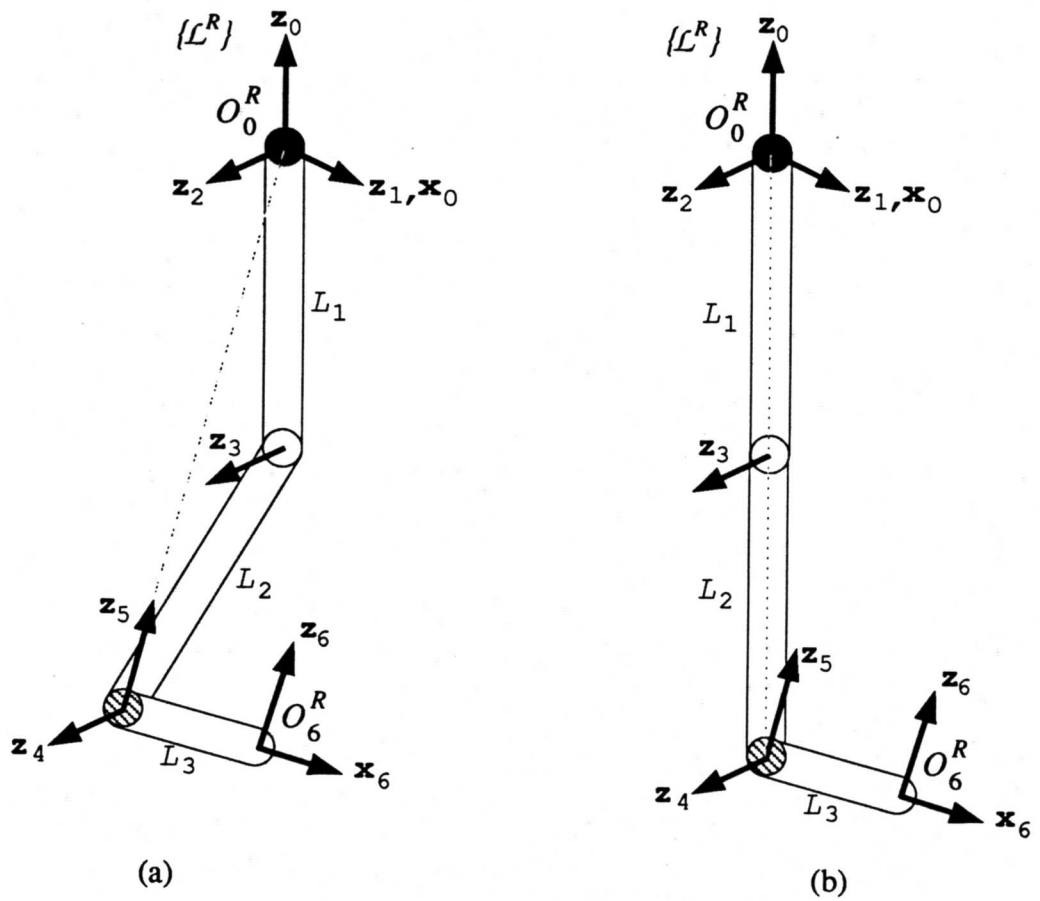

Figure 6: *The Singular Configurations of the Legs Model.*

It is observed from Figure 5a that the legs exhibit a symmetry along ${}^{B}\mathbf{z}_0$ of the body system. In a uniform walking sequence each leg assumes the same poses with respect to the body system periodically; this period is equal to half the walking cycle, that is, the time required for a single step sequence to be completed, and corresponds to a phase shift of $\pi/2$. Thus, only the inverse kinematics solution of one leg needs to be computed. The solution for the other leg can result by appropriate shifting of the obtained joint profile. This approach reduces the computational complexity to the half.

The first singular position for the human legs occurs when $\sin\theta_4 = 0$; a singularity may occur only when $\theta_4 = 0°$ since $0° \leq \mid \theta_4 \mid \leq 140°$. At this configuration, the human leg is fully extended. The second singularity takes place when the intersection point of the axes $\mathbf{z}_0$, $\mathbf{z}_1$, and $\mathbf{z}_2$, lies on the $\mathbf{z}_5$ axis; as a result, there exists an infinite number of solutions for θ_6. Finally, when axes $\mathbf{z}_0$ and $\mathbf{z}_2$ are aligned, θ_1 and θ_3 describe the same rotation and cannot be computed separately; one degree-of-freedom is thus lost. However, the joint limits in the motion about $\mathbf{z}_1$ dictate that $70° \leq \mid \theta_2 \mid \leq 130°$; therefore, this orientational singularity never occurs because of the joint limits. The singular configurations of the legs model are depicted in Figure 6.

3.3 The Human Arms Model

The human arms are modeled upon the realistic elbow geometry, that is, each joint exhibits limited rotational capabilities and the lengths L_1 and L_2 of the forearm and the upper arm, respectively, are not identical. The joint constraints reflect the limitations in the motion of the human arm, while the lengths L_1 and L_2 are determined from anthropometric data. The coordinate frames for the arms are depicted in Figure 7a.

The ${}^{A}\mathbf{z}_0$ axis for both arms points towards the direction of motion; this vector is always parallel to the ${}^{W}\mathbf{x}_0 - {}^{W}\mathbf{y}_0$ plane of the world coordinate system in walking applications, where no vertebrae flexion is present. Rotation about this axis corresponds to a shoulder *flexion*. The ${}^{A}\mathbf{x}_0$ axis point upwards, along the feet-head direction and is always parallel to the ${}^{W}\mathbf{z}_0$ axis of the world coordinate system in walking applications. The ${}^{A}\mathbf{y}_0$ axis completes the right hand frame. Typically, in a straight-line walking sequence, the orientation of $\{\mathcal{A}^R\}$ and $\{\mathcal{A}^L\}$ relative to the body and the world systems remains constant; changes in the direction of motion result from changes in the orientation of the body system. Rotations about axes ${}^{A}\mathbf{z}_1$, and ${}^{A}\mathbf{z}_2$, correspond to shoulder and elbow rotations, respectively. Rotations about ${}^{A}\mathbf{z}_3$, ${}^{A}\mathbf{z}_4$ and ${}^{A}\mathbf{z}_5$ correspond to a wrist yaw, pitch, and roll, respectively. The ${}^{A}\mathbf{z}_6$ axis lies along the fingers towards the reach direction and the ${}^{A}\mathbf{x}_6$ axis is perpendicular to the hand and points outwards.

The range of motion for each joint of the human arm model is depicted in Figure 7b, where $q_i = \theta_i$, $(i = 1, 2, \ldots, 6)$ denote the joint variables, and the superscripts R and L distinguish between the right and left arms, respectively. White dots in this figure indicate the values of the joint variables at the zero position, which occurs when the human model is standing (not walking). The direction of the arrows indicates how the same joint variable in the left and right arms varies in order to produce the same arm motion.

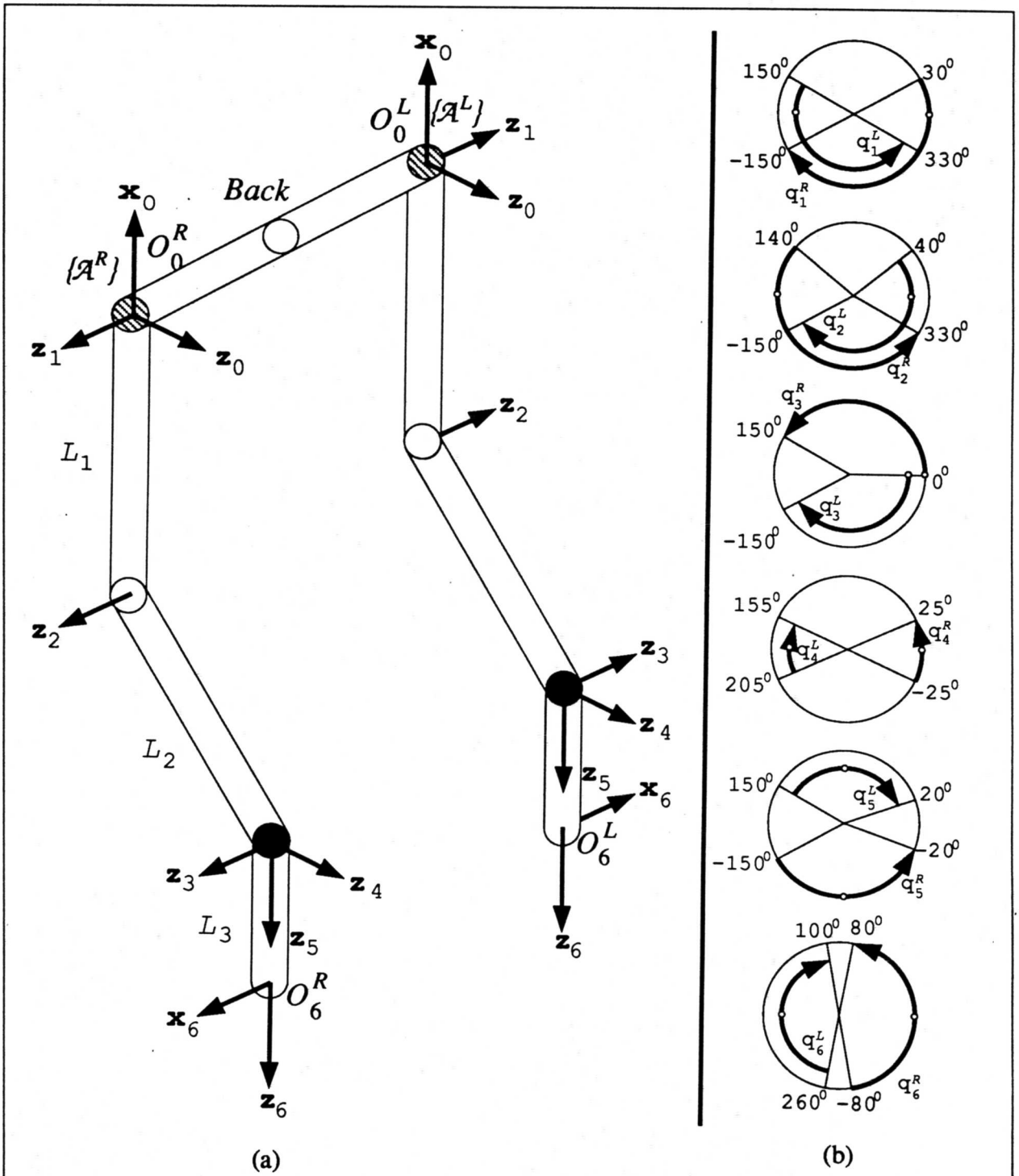

Figure 7: *(a) Definition of the Left and Right Arms Coordinate Systems. (b) The Range of Motion of the Arm Joints.*

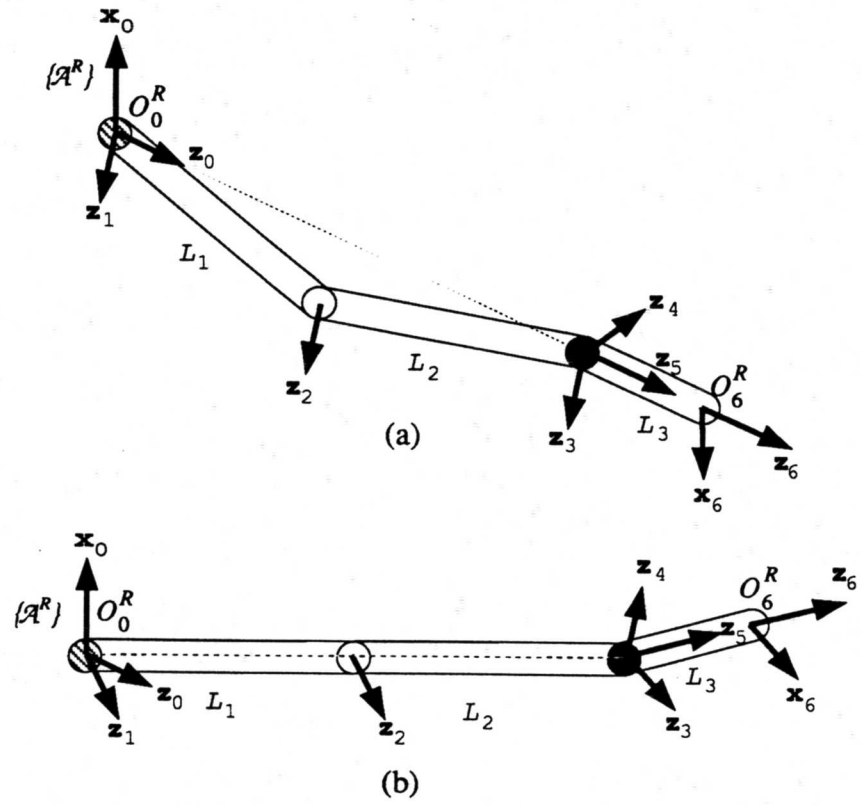

Figure 8: *The Singular Configurations of the Arms Model.*

The joint limits are employed to limit the solution space in the computation of the inverse kinematics solution for each arm at a desired pose. For example, since $0° \leq \theta_3^R \leq 150°$ ($-150° \leq \theta_3^L \leq 0°$) for the right (left) arm, $\sin\theta_3^R \geq 0$ ($\sin\theta_3^L \leq 0$) always; otherwise the arm will be forced to assume an abnormal position. Similarly, it follows that always $\sin\theta_5^R > 0$ ($\sin\theta_5^L < 0$).

It is observed from Figure 7a that the left hand exhibits a symmetry to the right hand along ${}^{\mathcal{B}}\mathbf{z}_0$ of the body system. In a uniform walking sequence each arm assumes the same positions periodically; this period is equal to half the walking cycle, that is, the time required for a single step sequence to be completed, and corresponds to a phase shift of $\pi/2$. The symmetry in the hands motion allows for the computation of the inverse kinematics solution of only one arm. The solution for the other arm can be obtained by appropriate shifting of the obtained joint profile. This approach reduces the computational complexity to the half.

The first singular configuration occurs when $\sin\theta_3 = 0$; since $0° \leq \mid \theta_3 \mid \leq 150°$, a singularity may occur only when $\theta_3 = 0°$. At this configuration the human arm is fully extended. The second singularity occurs when the intersection point of the axes $\mathbf{z}_3$, $\mathbf{z}_4$, and $\mathbf{z}_5$ lies on the $\mathbf{z}_0$ axis; one degree-of-freedom is then lost. Finally, when axes $\mathbf{z}_3$ and $\mathbf{z}_5$ are aligned, θ_4 and θ_6 describe the same rotation; one degree-of-freedom is thus lost. However, the joint limits in the motion about $\mathbf{z}_1$ dictate that $20° \leq \mid \theta_5 \mid \leq 150°$; therefore, this orientational singularity never occurs because of the joint limits. The singular configurations of the arms model are depicted in Figure 8.

4 Motion of the Human Model

In this section, the problem of moving the human model in space is addressed. First, the motion profiles for the arms and legs are described; then, the trajectory planning strategy is outlined, and finally, the computational complexity of the proposed approach is assessed.

4.1 The Walking Sequence

At all times in a walking sequence, at least one foot is in contact with the floor; during a brief phase, both feet are in contact with the floor. As walking is a cyclic activity, only the portion between two successive contacts of the heel of the same leg with the floor needs to be studied. The model employed herein utilizes the spatial and temporal characteristics of human walking to produce the joint parameters of the limbs.

The motion of the leg is comprised of four phases: The first phase describes the motion from the heel strike (HS) until the entire foot is in contact with the ground. During the second phase, the foot remains in full contact with the floor, while the other leg moves forward; the stance leg then carries the entire body weight. At the beginning of the third part, the heel loses contact with the ground, while at its end the toe leaves the floor; at the middle of this phase the other heel strikes the ground. During the fourth part, the swinging leg advances by a step length. Apart of the toes, the hip also follows a specific pattern of motion. The equations used to model this motion have been obtained from [23]. Once the joint coordinates for one leg have been computed these parameters can be determined for the other leg as well by a simple phase shift of $\pi/2$. The motion of the legs is depicted in Figure 9.

The motion of each arm during walking follows the motion of the opposite leg in the sense that when the right leg moves forward, the left arm also moves forward, and inversely. The torque applied to the *back* link is thus equal and opposite to the torque applied to the waist so that the main body does not rotate. Furthermore, each arm is moving opposite to the other arm so that the torque about the *back* link is zero.

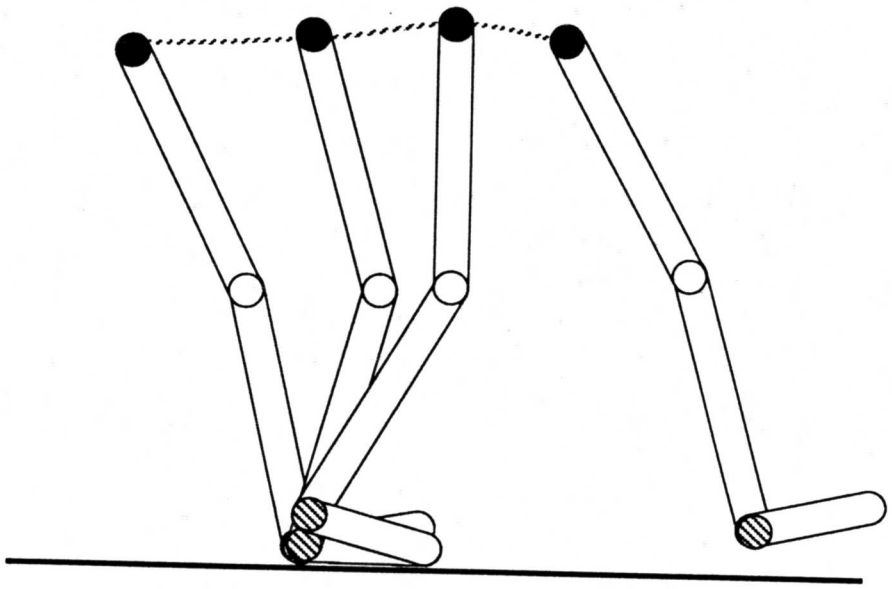

Figure 9: *Motion of the Legs During Walking.*

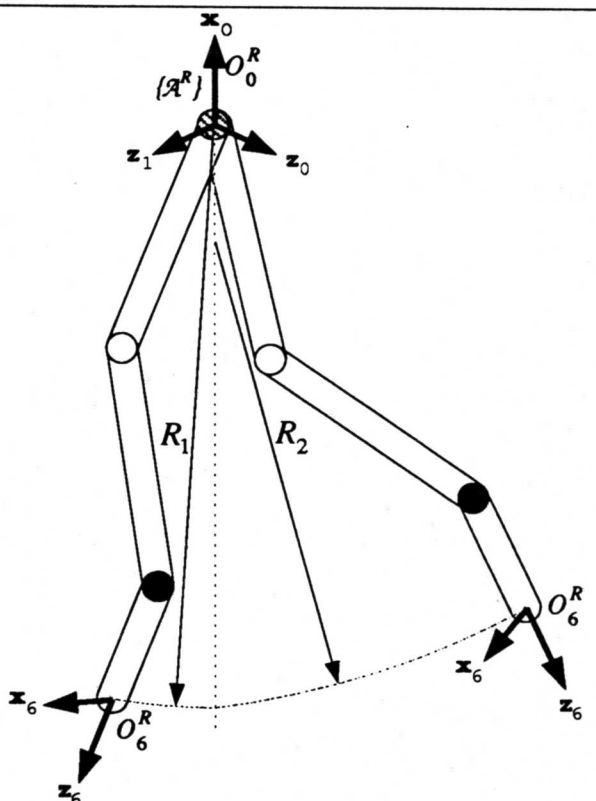

Figure 10: *Motion of the Arms During Walking.*

The motion profile of the arm with respect to the origin of the arm coordinate frame is depicted in Figure 10. The hand motion profile is completed in two phases: during the first phase the arm follows a circular arc centered at the shoulder with radius R_1 ($L_1 + L_2 < R_1 < L_1 + L_2 + L_3$), while during the second phase, the hand follows a circular arc centered at the middle of the upper arm with radius R_2 ($L_1/2 + L_2 < R_2 < L_1/2 + L_2 + L_3$). During the first part of the motion, the arm is almost stretched and the angle of the circular arc is at most 30°; during the second part, the elbow bends slightly and the angle of the circular arc typically varies from 30° to 45°. Once the joint coordinates for one arm have been computed these parameters can be determined for the other arm as well by a simple phase shift of $\pi/2$.

The motion profile of the limbs with respect to $\{\mathcal{B}\}$, for straight-line paths, or paths composed of straight line segments, is a function of the walking velocity only, for given body dimensions.

4.2 Trajectory Planning

The human model follows a predefined trajectory with respect to the constant world coordinate frame $\{\mathcal{W}\}$. This trajectory is specified as motion of the body coordinate frame $\{\mathcal{B}\}$; the motions of all other frames are performed with respect to this frame. A change in the direction of motion corresponds to a change in the orientation of $\{\mathcal{B}\}$, and inversely, changes in the direction of $\{\mathcal{B}\}$ result to changes in the walking direction of the human model. The head coordinate system $\{\mathcal{H}\}$ is assumed to follow these changes. The velocity of $\{\mathcal{B}\}$ with respect to $\{\mathcal{W}\}$ is the only parameter that needs to be specified for every straight line segment. Motion along more complex paths can also be simulated assuming that these are composed of many short linear segments; these segments can be designed to be arbitrarily small.

To compute the necessary joint displacements that generate a specific motion of each limb, the motion profile is divided into N segments (N usually varies form 30 to 100 for each step). Two approaches can then be followed: either the inverse kinematics solution is computed for each time instant or a kinematic control scheme is employed. The inverse kinematics approach, in general, requires more computations. Nevertheless, for the decoupled geometries of the human model, an analytic, closed-form solution always exists; furthermore, only one set of the eight possible needs to be computed.

The kinematic control strategy on the other hand may be quite expensive computationally and prone to computational errors since during walking the limbs move very close to singularities. This problem has been resolved by employing a singularity-robust resolved-motion rate kinematic control algorithm in the neighborhood of singularities [11, 24]. This approach always provides feasible solutions and guarantees smooth motion of the limbs at the neighborhood of singular positions. It has been shown that the computational cost associated with this control scheme is considerably lower than that of existing control algorithms because it exploits the decoupled nature of the arms and legs geometries.

FUNCTION	a	m	t
Arm Inverse Kinematics	31	45	26
Leg Inverse Kinematics	32	38	29
Singularity-Robust Arm Jacobian	28	66	12
Singularity-Robust Leg Jacobian	28	66	12
Inverse Arm Jacobian	12	24	11
Inverse Leg Jacobian	12	24	11

Table 3: *Computational Load at Every Time Instant.*

4.3 Computational Complexity

The computational complexity at every time instant is summarized in Table 3 when the inverse kinematics are computed and when a kinematic control strategy is employed. These results indicate that it is preferable to employ the inverse kinematics strategy for walking applications. This is not, in general, the case in robotic applications. The motion of the limbs, nevertheless, close to the singularities dictates the use of singularity-robust inverse Jacobians which, although stable, are more computationally expensive.

5 Example

In this section, the behavior of the presented model is illustrated through an example. Specifically, the human model is ordered to walk in a straight line. The present application employs ray tracing to graphically represent the motion of the human model in the scene. The links of the human model are represented by ellipsoids, the number of which depends on the degrees-of-freedom in the kinematic representation, while their shape reflects the dimensions according to anthropometric data. Specifically, the model is composed of sixteen ellipsoids, that is, three for each limb, one for the waist, one for the chest, one for the back, and one for the head [25].

The following assumptions have been made:

- Only one light source is defined and used. Currently, the light source coincides with the camera. The eye can thus perceive only these objects which are illuminated.
- Both the virtual camera and the light source are modeled upon the pinhole camera; that is, they are dimensionless points [26].
- The objects in the scene are assumed to be perfect surfaces, in the sense that they scatter light equally in all directions.
- The implemented ray tracer calculates only first-order rays, by employing the *Lambertian diffuse reflectance model.*
- No antialiasing methods are used; only one ray is thus cast through each pixel.

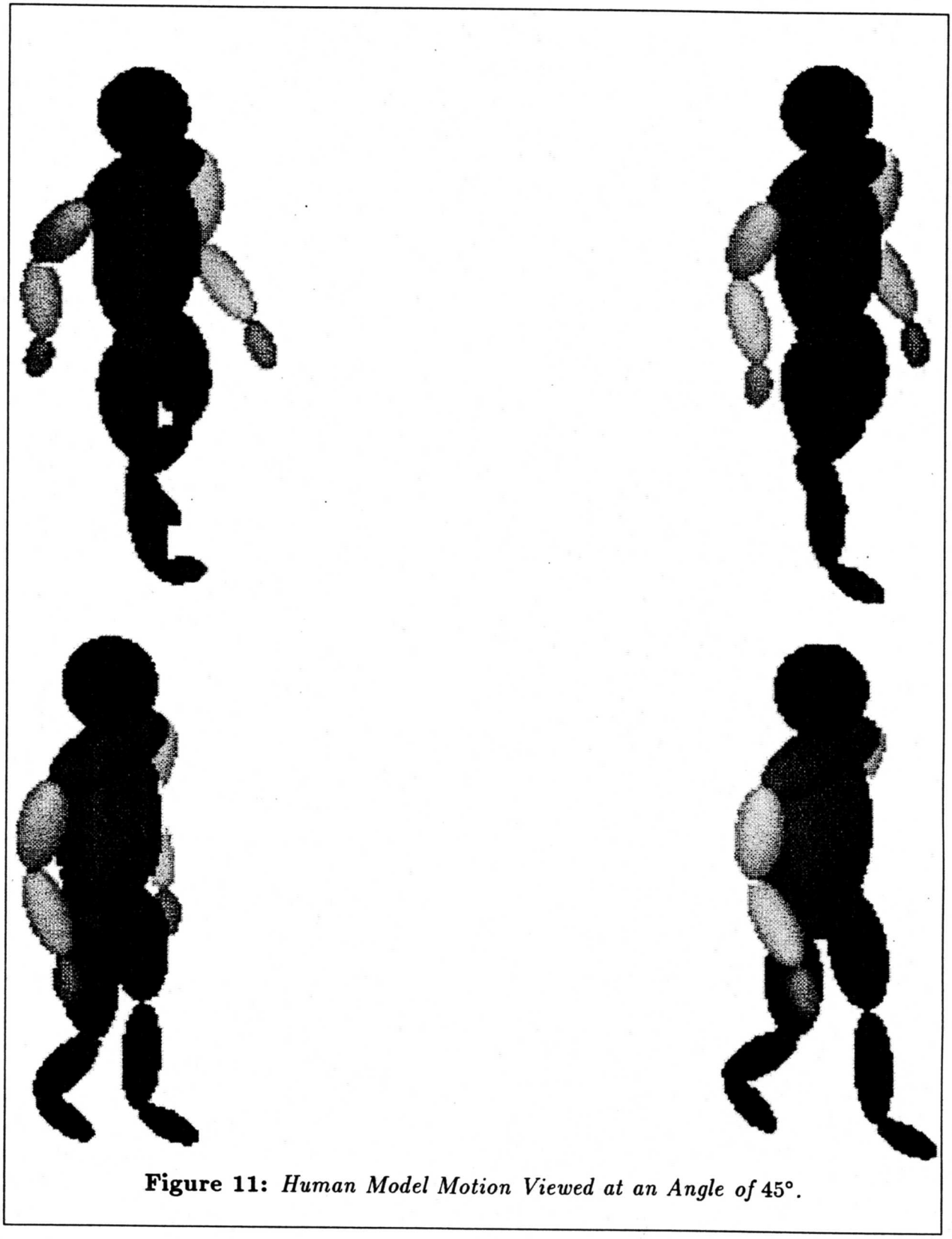

Figure 11: *Human Model Motion Viewed at an Angle of* 45°.

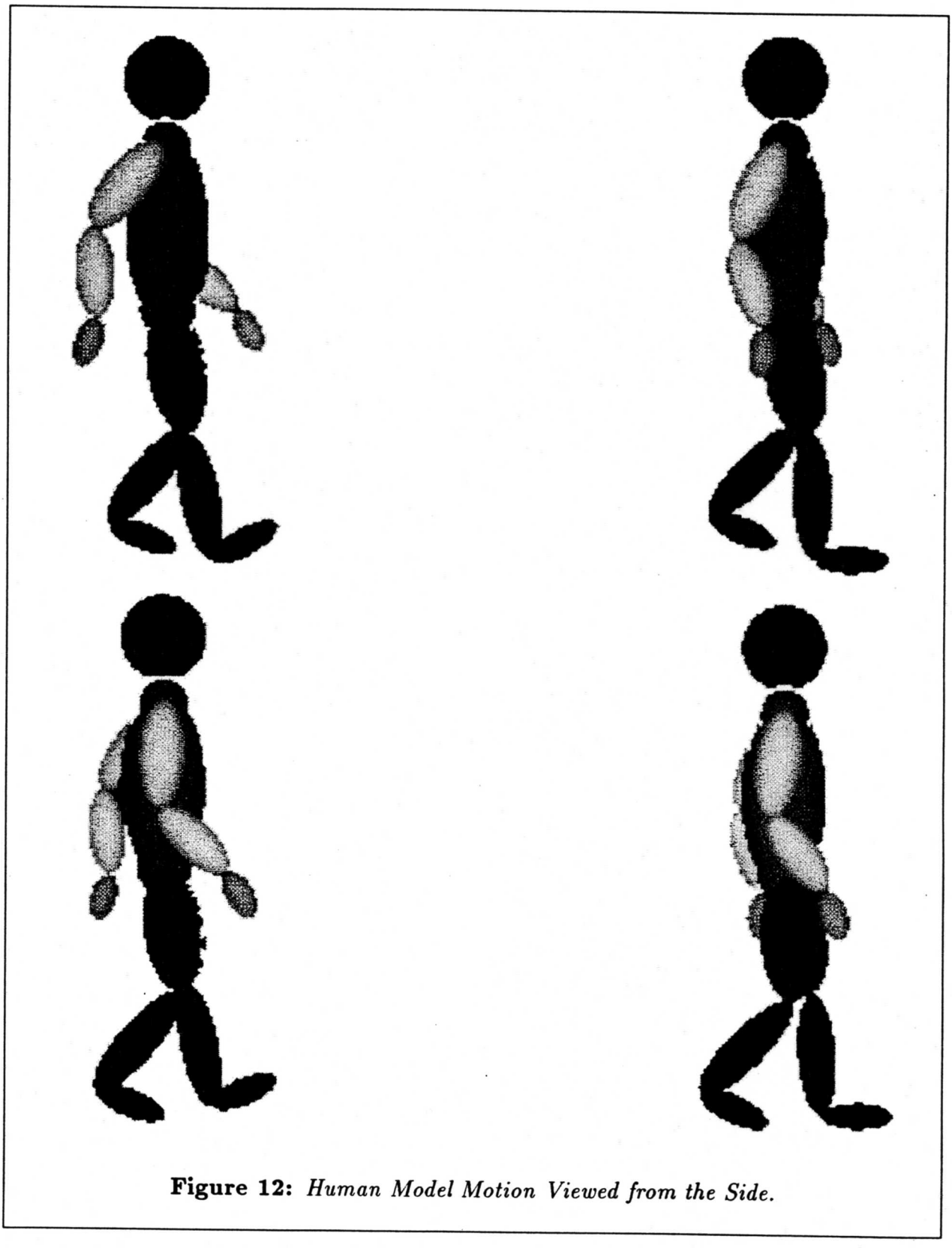

Figure 12: *Human Model Motion Viewed from the Side.*

The poses (position and orientation) of the ellipsoids are calculated by the general animation model. To produce an animating sequence, the pose of each ellipsoid is computed and input to the ray tracing program. Hidden surface removal and shading are accomplished with ray tracing. The motion of the human model is smooth, and satisfies the imposed joint constraints *and* the floor constraints (that is, there is no foot penetration on the floor). The complete algorithm for the human model motion is implemented in the C++ programming language [27]. Figures 11, and 12 depict two different perspectives of the motion from different viewing angles.

6 Conclusions

In this paper, the problem of kinematic human modeling has been investigated. A kinematic model that employs two classes of optimal articulated geometries to model the limbs, has been developed. The decoupling properties of the elbow and dual-elbow geometries have been utilized to create closed-form, analytic inverse kinematic solutions. Furthermore, the symmetry in the motion of the two pairs of limbs during walking has been exploited to reduce the computational time in half. An integrated ray tracing and rendering algorithm has been created to accompany the main algorithm and to present realistic motion in screen.

In order to extend the contributions of this investigation, the following research directions are suggested:

- Further research on the study of human motion.
- Study of different types of motion of the human model in space.
- Customization and classification of motion patterns.
- Investigation of motion planning strategies of the human model in space and path optimization for complex environments.
- Development of a human model which accounts for the dynamic interactions between the distinct subsystems that compose it.

Continuing research along these lines will reveal the full potential of the optimal geometries in human modeling, and accelerate their utilization in computer animation applications.

References

[1] N. Magnenat Thalmann and D. Thalmann. *Synthetic Actors in Computer-Generated 3-D Films.* Springer-Verlag, New York, 1990.

[2] A. Watt and M. Watt. *Advanced Animation and Rendering Techniques: Theory and Practice.* Addison-Wesley, New York, NY, 1992.

[3] P.M. Isaacs and M.F. Cohen. "Controlling Dynamic Simulation with Kinematic Constraints, Behavior Functions and Inverse Dynamics". *Computer Graphics*, 21(4):215–224, July 1987.

[4] P.M. Isaacs and M.F. Cohen. "Mixed Methods for Complex Kinematic Constraints in Dynamic Figure Animation". *Visual Computer*, 4:296–305, 1988.

[5] C.W.A.M. van Overveld. "A Technique for Motion Specification in Computer Animation". *Visual Computer*, 6:106–116, 1990.

[6] L. Silverberg and J.R. Gardiner. "Simulation of the Mechanics of Water-Skier Motion". *Mathematics and Computers in Simulation*, 34:163–181, 1992.

[7] J.U. Korein and N.I. Badler. "Techniques for Generating the Goal-Directed Motion of Articulated Structures". *IEEE Computer Graphics and Applications*, pages 71–81, November 1982.

[8] B. Arnaldi, G. Dumont, G. Hegron, N. Magnetat-Thalman, and D. Thalmann. "Animation Control with Dynamics". In *State of the Art in Computer Animation*, pages 113–123. Springer-Verlag, Berlin, 1989.

[9] P. Lee, S. Wei, J. Zhao, and N.I. Badler. "Strength Guided Motion". *Computer Graphics*, 24(4):253–262, August 1990.

[10] D.M. Emiris and V.D. Tourassis. "Workspace Analysis of Realistic Elbow and Dual-Elbow Robot Manipulators". *Mechanism and Machine Theory*, 28(3):375–396, May 1993.

[11] D.M. Emiris. *Kinematic Analysis, Evaluation and Control of Dual-Elbow Robotic Manipulators.* PhD thesis, Department of Electrical Engineering, University of Rochester, Rochester, NY, May 1991.

[12] D.M. Emiris and V.D. Tourassis. "Closed-Form Inverse Kinematics Solution for a Dual-Elbow Manipulator". In *Proceedings of the Twelfth IASTED International Symposium on Robotics and Manufacturing*, pages 70–74, Santa Barbara, CA, November 13–15, 1989.

[13] B. Paden and S. Sastry. "Optimal Kinematic Design of 6R Manipulators". *International Journal of Robotics Research*, 7(2):43–61, Spring 1988.

[14] V.D. Tourassis and D.M. Emiris. "A Comparative Study of Ideal Elbow and Dual-Elbow Robot Manipulators". *Mechanism and Machine Theory*, 28(3):357–373, May 1993.

[15] C. Lanczos. *Applied Analysis.* Prentice Hall, Englewood Cliffs, NJ, 1956.

[16] M. Uchiyama. "A Study of Computer Control of Motion of a Mechanical Arm". *Bulletin of the Japanese Society of Mechanical Engineering*, 22(173):1640–1647, November 1979.

[17] B. Paden and S. Sastry. Geometric interpretation of mathematical singularities. Technical Report UCB/ERL M84/76, University of California, Berkeley, September 1984.

[18] V.D. Tourassis. "Principles and Design of Model–Based Controllers". *International Journal of Control*, 47(5):1267–1275, May 1988.

[19] S. Desa and B. Roth. "Mechanics: Kinematics and Dynamics". In G. Beni and S. Hackwood, editors, *Recent Advances in Robotics*, pages 71–130. John Wiley & Sons, New York, NY, 1985.

[20] D.M. Emiris and V.D. Tourassis. "The Reachability and Dexterity of Elbow and Dual-Elbow Robot Manipulators". *Journal of Robotic Systems*, 9(8):1021–1041, 1992.

[21] D.M. Emiris and V.D. Tourassis. "Analysis of the Effects of Manufacturing Errors on the Accuracy of Dual-Elbow and Elbow Manipulators". *Mechanism and Machine Theory*, 1993. (in press).

[22] R. Vijaykumar, K.J. Waldron, and M.J. Tsai. "Geometric Optimization of Serial Chain Manipulator Structures for Working Volume and Dexterity". *International Journal of Robotics Research*, 5(2):91–103, Summer 1986.

[23] R. Boulic, N.M. Thalmann, and D. Thalmann. "A Global Human Walking Model with Real–Time Kinematic Personification". *Visual Computer*, 6:344–358, 1990.

[24] D.M. Emiris and V.D. Tourassis. "Singularity–Robust Decoupled Control of Dual-Elbow Manipulators". *Journal of Intelligent and Robotic Systems*, 1993. (in press).

[25] D.F. Rogers and A. Adams. *Mathematical Elements for Computer Graphics.* McGraw-Hill, New York, NY, 1990.

[26] F.S. Hill Jr. *Computer Graphics.* Macmillan Company, New York, NY, 1990.

[27] C.D. Watkins, S.B. Coy, and M. Finlay. *Photorealism and Ray-Tracing in C.* Prentice Hall, Englewood Cliffs, NJ, 1992.